JOURNAL OF COATING TECHNOLOGY AND INNOVATION
Apr-Jun 2024, VOL. 2, ISSUE 2, pp. 19-28
https://doi.org/10.61577/jcti.2024.100008

RESEAPRO JOURNALS

ORIGINAL ARTICLE

OPEN ACCESS

Electrophoretic deposition of novel 2D MXene for anti-corrosion application

N Usha Kiran[1], Ghrutanjali Sahu[2], Sriparna Chatterjee[3], and Laxmidhar Besra[4]

[1,2,3,4]Department of Materials Chemistry, CSIR-Institute of Minerals and Materials Technology, Odisha, India
[3,4]Academy of Scientific and Innovative Research (AcSIR), Ghaziabad, India

ABSTRACT

Corrosion is a persistent problem that can cause significant damage to structural components and safety hazards, making it an important concern for many industries due to reduced durability and increased maintenance costs. This process is caused by a variety of factors, including exposure to moisture, chemicals, and a non-inert environment. Therefore, finding effective ways to prevent or slow down corrosion is crucial. Several protective methods have been utilized to prevent metals from severe degradation. In this regard, two-dimensional Titanium Carbide ($Ti_3C_2T_x$), known as 'MXene', represents a new class of material with improved functionality, and offers great promise because of its extraordinary mechanical, electrical, and electrochemical properties. Despite the widespread use of $Ti_3C_2T_x$ MXene in energy storage, catalysis, purification, and electromagnetic interference shielding, their anticorrosion performance has received relatively little investigation. This article reports the electrophoretic deposition (EPD) of $Ti_3C_2T_x$ MXene on copper substrate. The synthesis of $Ti_3C_2T_x$ MXene involves the typical wet chemical etching of the silicon layer in HF/H_2O_2 etchant solution from titanium silicon carbide (Ti_3SiC_2) – the most common MAX phase. The precursor Ti_3SiC_2 MAX phase was also synthesized by heating at high temperatures. For EPD, a stable colloidal suspension of 1wt % $Ti_3C_2T_x$ MXene was prepared in 1-methyl-2-pyrrolidone, and coating was done at an applied voltage of 150 V in the deposition time range of 5s to 60s, using a DC power source. The desired uniform coating with varying thicknesses was optimized for further characterization such as X-ray diffraction (XRD), Scanning Electron Microscopy (SEM), etc. Electrochemical measurements revealed a significant increase in resistance of the nanostructured coating against corrosion with 99.8% inhibition efficiency. This work provides a platform for other MXene compositions that may be used to further broaden the scope of this investigation.

KEYWORDS

MAX phase; MXene; Electrophoretic deposition; Corrosion

ARTICLE HISTORY

Received 30 May 2024;
Revised 17 June 2024;
Accepted 25 June 2024

Introduction

Corrosion refers to the gradual deterioration of materials, typically metals, due to their interaction with oxygen, moisture, salts, air-borne pollutants like chlorides and sulfides, changes in temperature in electronic components, and other aggressive chemicals. This weakens the material, leading to structural failures and safety hazards [1]. This process involves a chemical or electrochemical reaction that transforms the material/metal into its more stable form. Corrosion costs India $26.1 billion, which is 2.4% of the country's GDP. Out of this, $9.3 billion could be saved, which is 35% of the direct corrosion cost. Additionally, the indirect cost of corrosion is $39.8 billion [2]. Corrosion can occur in many different forms, including uniform corrosion, pitting corrosion in aluminium structures, electrochemical & fretting corrosion in electronics, galvanic corrosion in the automotive industry, etc. In recent years, several methods have been developed and implemented to improve anti-corrosion performance. Major corrosion prevention strategies include the use of corrosion-resistant materials, cathodic protection, the application of protective organic and inorganic coatings, etc. [3]. Although organic coatings are preferable due to high efficiency and low cost, the major disadvantage of this is they quickly develop micropores and these pores allow the electrolyte to rapidly get into the metal [4]. Therefore, researchers are currently working on developing a corrosion inhibitor that is much more effective. In the search for more reliable materials to deliver enhanced physicochemical properties of the coatings, two-dimensional (2D) nanomaterials have shown a growing interest in this field. Graphene oxide (GO), a modern 2D nanomaterial shows exceptional anti-corrosion properties due to its impermeability to gases, liquids, and ions [5-7]. However, GO coating is less stable as it readily absorbs moisture from the environment where the water molecule can pass through the graphene nano-channels, create leakage pathways, and potentially promote corrosion of underlying metals [8,9]. In addition, GO with decreased electrical conductivity can be problematic for applications where electrical conductivity is crucial.

Recently, researchers at Drexel University discovered a family of new 2D transition metal carbides, nitrides and carbonitrides called "MXenes" in 2011 which can be synthesized by selective etching of certain atomic 'A' layers (Group-13 & 14 elements) from their corresponding three-dimensional (3D) layered precursor MAX phase [10]. To date, >150 MAX phase compositions and approximately 50 MXenes have been experimentally synthesized [11]. Among different types of experimentally proven MXenes, more than 70% of the research has been done on $Ti_3C_2T_x$ MXene alone as it shows great potential towards various applications. This novel material also shows great potential as a coating material due to its unique properties such as unique layered structure,

***Correspondence:** Dr. Laxmidhar Besra, Department of Material Chemistry, CSIR-Institute of Minerals & Materials Technology, Bhubaneshwar, India, 751013, Tel/ Fax: +91 674 2379244, e-mail: ldbesra@immt.res.in

lightweight, high optical transparency, negative zeta potential, high electrical conductivity, adjustable band-gap, tunable surface, and excellent mechanical strength [12]. It is used as an anode coating material of a lithium-ion battery to improve its performance and stability. It can also be applied as a thin coating layer which possess a "nano-scale barrier effect" that creates a "labyrinth effect", prolonging the penetration path of destructive elements into the coatings and metal substrates [13].

Various coating technologies, such as spray coating, spin coating, dip coating, chemical vapour deposition (CVD), electrophoretic deposition (EPD), and inkjet printing, can be used to apply MXene onto different surfaces, each offering unique advantages and disadvantages based on the intended application and desired coating properties (Figure 1) [14].

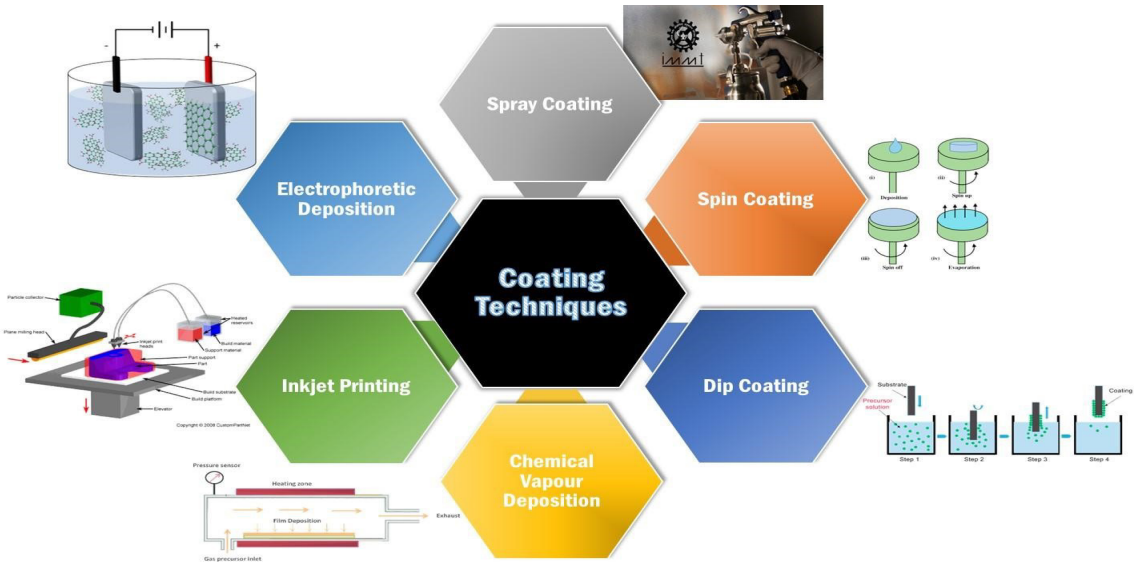

Figure 1. Different coating techniques used for the coating of 2D MXenes.

Yan et al. investigated the corrosion resistance of Q345 steel coated with a Ti_3C_2 MXene and epoxy resin composite using a coater [15]. The steel was tested by immersing it in 3.5% NaCl for 96 hours. Adding 1 wt% Ti_3C_2 to the epoxy, reduced water absorption to 0.23 wt% from 0.96 wt% in pure epoxy. This significantly decreased metal corrosion after 15 days. Similarly, Zhao et al. developed air-stable, oxidation-resistant $Ti_3C_2T_x$ MXene nanosheets functionalized with an ionic liquid (IL), which significantly enhanced the anticorrosion performance of waterborne epoxy (WEP) coatings. The IL@MXene-WEP coatings showed a 1-2 orders of magnitude increase in impedance and exhibited excellent self-healing properties, reducing local corrosion in a 3.5% NaCl solution [16]. In another study, Li et al. improved the anticorrosion performance of waterborne epoxy coatings by adding L-Cysteine functionalized $Ti_3C_2T_x$ MXene nanosheets. After 30 days in 3.5 wt% NaCl, the fMX/WEP coatings showed significantly higher low-frequency impedance and lower corrosion rates compared to the blank WEP, demonstrating enhanced protection [17]. $Ti_3C_2T_x$ MXene coatings were prepared by Shi et al. on X70 steel using a simple spin coating method, revealing excellent corrosion protection through a diffusion barrier. A significant positive shift of 170 mV in E_{corr} and a decrease in I_{corr} to 1.5 μA·cm^{-2} were observed in the MXene-coated steel, indicating enhanced corrosion resistance compared to uncoated steel after 30 minutes of immersion [18]. Despite these coating methods, exploring an efficient and cost-effective coating method for industrial applications is an ongoing challenge. In this regard, Electrophoretic deposition (EPD) has gained significant attention in recent years for its ability to produce high-quality, uniform coatings on complex-shaped substrates with excellent adhesion and scalability to large product sizes.

Electrophoretic Deposition (EPD) of MXene: Literature Review

Electrophoretic deposition (EPD) is a technique used to deposit particles such as ceramics, metals, and polymers onto a substrate by applying an electric field. A typical EPD system consists of a power supply, a conductive substrate, a counter-electrode, and a stable suspension of charged particles. When voltage is applied, active material particles from the liquid dispersion are deposited onto the substrate. This technique has also been applied to the deposition of 2D materials such as MXene and graphene [7]. $Ti_3C_2T_x$ MXene possesses a negative surface charge (around -40 mV). MXene flakes can be dispersed in a suitable solvent and a voltage is applied to the substrate, causing the MXene flakes to migrate towards their respective electrode and deposit on the surface. One application of MXene coatings using EPD is in the fabrication of supercapacitor electrodes. The MXene-coated electrodes exhibit high capacitance, fast charge/discharge rates, and excellent cycling stability, making them promising candidates for energy storage applications [19,20]. MXene coatings have also been explored for water purification applications. Deng et al. prepared a 575 cm² MXene membrane using EPD in 10 minutes, achieving ~99.5% Na+ ion rejection, compared to ~94.7% for the same thickness membrane made with vacuum-assisted filtration [21]. MXene coatings have also been shown to exhibit antibacterial properties which can prevent implant-associated infections. Jang et al. reported the improvement of the osteoinductivity of Ti by depositing a $Ti_3C_2T_x$ MXene coating on the material surface via the EPD technique [22]. The EPD technique is a promising method for applying MXene coatings to various substrates for diverse applications. A statistical approach conducted by Namvari et al.

https://doi.org/10.61577/jcti.2024.100008

in Scopus search using the terms "electrophoretic," "deposition," and "MXene" reveals a notable rise in publications across multiple fields, with significant growth observed up to December 2023 [23]. However, there is a noticeable lack of coverage in the literature regarding electrophoretically deposited MXene for anti-corrosion application. By addressing this gap, researchers can advance our understanding of corrosion mitigation strategies and contribute to the development of advanced materials coating for diverse industrial applications.

In this study, the $Ti_3C_2T_x$ MXene was produced from conventionally synthesized (pressureless sintering) Ti_3SiC_2 MAX phase by HF etching. The XRD analysis confirms the change in d-spacing of $Ti_3C_2T_x$ MXene with respect to its bulk counterpart. The EPD technique was used to coat $Ti_3C_2T_x$ MXene onto a copper substrate. Various deposition parameters were optimized for uniform coating formation. The morphological analysis showed a homogeneous and uniform coating of $Ti_3C_2T_x$ MXene on the substrate. The Tafel measurements exhibited excellent corrosion inhibition efficiency in comparison to the bare substrate. This work will be an added benefit to the electronic industries where electrical conductivity and electromagnetic interference (EMI) shielding is an important factor. As $Ti_3C_2T_x$ MXene exhibits exceptional shielding ability, the components inside the device could be coated with MXene material to prevent electrochemical corrosion and restrict EMI without change in the property of electrical conductivity [24].

Experimental Procedure

Synthesis of high-pure Ti_3SiC_2 MAX phase

The synthesis of high-pure Ti_3SiC_2 MAX phase was obtained as reported in our previous work [25]. In short, for the synthesis of high-pure Ti_3SiC_2 MAX phase, the raw materials of elemental Ti (200 µm, 99% purity, John Baker Inc., Colorado, USA), Si (250 µm, 99% purity, Central Drug House Pvt. Ltd., India) and C (100 µm, 99.5% purity, Central Drug House Pvt. Ltd., India) were taken in a poly-propylene bottle at a molar ratio of 3:1.2:2. The powder mixture was mixed homogeneously for 12 h in ethanol using 2 mm zirconia balls (ball to powder ratio ~10:1). The milled powder was then vacuum dried followed by cold pressing at room temperature into cylindrical pellets of 20 mm diameter and 2 mm thickness on application of 100 $kgcm^{-2}$ uniaxial pressure. The compact mixture was then heat treated at 1400 °C for 140 minutes in an argon atmosphere with a heating rate of 10 °C/min. The as prepared sample looks grey in colour. The synthesized pellet was crushed to powders for further characterization and for the fabrication of 2D Ti_3C_2T MXene nanosheets.

Synthesis of $Ti_3C_2T_x$ MXene (multi-layer) by wet chemical etching

The synthesis of 2D $Ti_3C_2T_x$ MXene nanosheets was obtained as reported in our previous work [26]. For the fabrication of extra-ordinary multi-layer $Ti_3C_2T_x$ MXene nanosheets, a mixture of HF (Hydrofluoric acid, 40% assay, FINAR Chemicals Pvt. Ltd.), India and H_2O_2 (Hydrogen peroxide, 30% assay, Central Drug House Pvt. Ltd., India) was prepared initially by mixing 5 ml of H_2O_2 (35 wt. %) and 50 ml of HF (40 wt. %) followed by stirring for 15 minutes in an ice-bath (≤ 5 °C). Then, 3 g of grayish Ti_3SiC_2 MAX powder was slowly added to the solution mixture and stirred for 2 h in ice-cold condition. The reaction mixture was then placed in an oil bath, pre-heated at 40 °C, and stirred further for 48 h. Then, the product was recovered by centrifugation on repeatedly washing with DI water (Milli-Q Integral 3 system, Millipore, USA) till the pH gets neutral. Finally, it was washed twice with ethanol and acetone and dried in vacuum at 100 °C to obtain multi-layer $Ti_3C_2T_x$ MXene powder.

Due to the susceptibility of single or few-layer MXene to oxidation, this work focuses on synthesizing and coating multilayer MXene on the desired substrate to ensure long-term stability and corrosion prevention in a corrosive environment [27]. For a detailed understanding of the researchers, optimization of process parameters for high quality multi-layer $Ti_3C_2T_x$ MXene nanosheets has been discussed in section 3.2 of this article.

Electrophoretic deposition of 2D $Ti_3C_2T_x$ MXene

For electrophoretic deposition (EPD), the $Ti_3C_2T_x$ MXene nanosheets thus prepared were first dispersed in 1-methyl-2-pyrrolidone by ultrasonication for about 15 mins. The multi-layer MXene powder was completely dispersed, forming a black suspension. Since the MXene suspension is negatively charged, an anodic EPD process was used for coating of MXene nanosheets. The copper sheet (purity: 99.99%), obtained from Rashmita Traders (Bhubaneshwar, Odisha, India) was cut into strips of finite dimension (5 cm × 2 cm). Then, the strips were polished with 220 grit silicon carbide paper and subjected to ultrasonic cleaning for 30 minutes using a combination of distilled water and acetone before coating. The copper strip served as the deposition electrode (anode) and a graphite strip (5 cm × 3 cm) was used as the cathode. The electrodes were hung vertically into the MXene suspension contained in a glass beaker at a gap of 2 cm from each other. A constant DC voltage of 150 V was applied to the suspension with a variable deposition time (5–60 sec), utilizing a source meter (Model-2410, Keithley Instruments Inc., Cleveland, OH, USA). The samples coated using the optimized parameters of 150V and 45 seconds were found to be the best, resulting in a thin and uniform deposition. The coated green samples were vacuum-dried overnight and were used for further characterization.

Characterization

The crystal structure and phase identification of the products were obtained by x-ray diffraction (XRD) (X'pert PRO, Malvern PANalytical, Netherlands) using Cu-Kα as x-ray source. The percentage composition of crystallographic phases such as Ti_3SiC_2, TiC, and Ti_5Si_3 in all the samples was determined through the integration of X-ray diffraction (XRD) peak intensities using the below equation:

$$Phase\ (\%) = \frac{Ix}{It} \quad [1]$$

Where, 'I_x' represents the integrated area of the most intense peak corresponding to the phase under analysis [In this work: Ti_3SiC_2 (104), TiC (200), Ti_5Si_3 (211)], while 'I_t' stands for the cumulative sum of the integrated areas of the most intense peaks of all currently present representative phases. Microstructural characterization was done using a field-emission scanning electron microscope (FESEM)

https://doi.org/10.61577/jcti.2024.100008

equipped with an Energy Dispersive X-ray Spectrometer (EDX) (Supra-55, Zeiss instruments, Jena, Germany). Raman spectrometer (InVia Renishaw, Gloucestershire, UK) equipped with an air-cooled CCD (Charge Coupled Device) detector was used as a tool to determine the signs of oxidation and degradation of exfoliated MXene nanosheets. NIR laser beam of excitation wavelength 785 nm with an exposure time of 100 seconds was used in the analysis. Electrochemical investigations were performed using CHI-660E electrochemical workstation (Austin, TX, USA) instrument in 3.5% sodium chloride (NaCl) solution at room temperature.

Results and Discussion

Effect of process parameters on the synthesis of Ti_3SiC_2 MAX phase

To ascertain the crystallinity and phase purity of Ti_3SiC_2 MAX phase, fine powders of titanium, silicon, and carbon are mixed in 3 different stoichiometric ratios viz. 3:1:2, 3:1.1:2 and 3:1.2:2. Figures 2(a), 2(b), and 2(c) represent the X-ray diffraction pattern of formation of Ti_3SiC_2 MAX phase with varying concentration of 'Si' in 3:1:2, 3:1.1:2 and 3:1.2:2, respectively at different temperatures (1300 °C to 1400 °C) and time (1-2 hr).

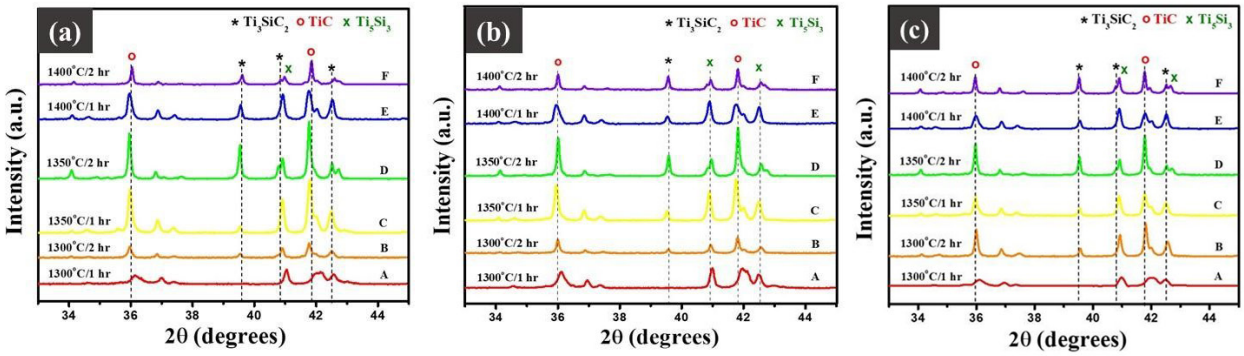

Figure 2. X-ray diffraction pattern of all the heat-treated samples showing Ti_3SiC_2 MAX phase, TiC and Ti_5Si_3 at different intensities with respect to varying temperature, time at a molar ratio: (a) 3:1:2, (b) 3:1.1:2 and (c) 3:1.2:2.

During the sintering process, the powder mixture is heated at a heating rate of 10 °C/min in argon atmosphere. The presence of diffraction lines at 2θ ~ 9.9°, 39.5°, 40.8°, and 42.5° confirms the formation of Ti_3SiC_2 MAX phase in all the plots with different concentrations of 'Si' taken. (JCPDS ref. code: 03-065-3559). The peak at 2θ ~36° and ~41.8° confirms the formation of TiC as an intermediate phase with an increase in peak intensity up to 1350 °C for all the plots. The diffraction lines emerged at the angle 40.8° and 42.5° corresponds to intermediate Ti_5Si_3, since the corresponding plane shows the major peak intensity according to the JCPDS database no.: 00-039-1283. To minimize the formation of impurities, 0.1 and 0.2 molar excess silicon is added to compensate for the loss of silicon at high temperatures i.e. at 1400 °C. The increase in I_{TC}/I_{TSC} ratio to 0.65 with 3:1.2:2 molar concentration of elemental Ti:Si:C powder in Figure 2(c) confirms the formation of Ti_3SiC_2 MAX phase where 'Si' plays an important role during the synthesis (Table 1).

Table 1. Phase composition of different crystallographic phases formed in all the samples that were heat treated at varying temperatures (1300-1400 °C), time (1-2 hr) and concentration of 'Si' (1, 1.1 and 1.2).

Ti/Si/C powder mixture ratio	Heating temperature (°C)	Heating time (min)	Detected crystallographic phases (%)		
			TiC	Ti_3SiC_2	Ti_5Si_3
3/1/2	1300	60	44.9	2.4	52.7
	1300	120	51.1	14.9	34.0
	1350	60	57.0	6.8	36.1
	1350	120	59.7	22.1	18.2
	1400	60	41.7	21.4	36.9
	1400	120	58.3	23.4	18.3
3/1.1/2	1300	60	48.9	1.4	49.8
	1300	120	56.1	13.4	30.5
	1350	60	51.3	12.1	36.6
	1350	120	56.6	23.7	19.8
	1400	60	39.2	14.4	46.4
	1400	120	51.9	25.1	23.0
3/1.2/2	1300	60	48.1	2.9	49.0
	1300	120	53.2	12.8	34.0
	1350	60	44.8	15.3	40.0
	1350	120	54.2	25.0	20.8
	1400	60	35.1	18.4	46.4
	1400	120	41.5	29.7	28.8

https://doi.org/10.61577/jcti.2024.100008

The percentage composition of crystallographic phases such as Ti_3SiC_2, TiC and Ti_5Si_3 in all the samples were determined (Table 1) through the integration of X-ray diffraction (XRD) peak intensities using equation-1. Here, I_x is replaced with I_{TSC} which represents the integrated diffraction peak intensity of the Ti_3SiC_2 phase along the (104) plane, I_{TC} represents the integrated diffraction peak intensity of TiC phase along the (200) plane, and I_{TS} represents the integrated diffraction peak intensity of Ti_5Si_3 phase along the (211) plane [28].

These findings suggest that prolonged heating at higher temperature (1400 °C) contributes to the progressive formation of the Ti_3SiC_2 MAX phase, a crucial observation for optimizing synthesis conditions. With subsequent optimization, high-pure Ti_3SiC_2 MAX phase was synthesized at 1400 °C for 140 minutes in an argon atmosphere with a heating rate of 10 °C/min (see section 2.1).

Optimization of $Ti_3C_2T_x$ MXene synthesis using different etchant concentrations

This section explores the disadvantages associated with the use of high and low etchant concentrations in MXene synthesis, highlighting material quality issue. This helps the researchers to minimize the limitations and enhance the MXene synthesis efficiency.

High etchant concentration

Higher concentrations of HF expedite the etching process, accelerating the removal of silicon layers from the Ti_3SiC_2 MAX phase and consequently reducing the synthesis time required for $Ti_3C_2T_x$ MXene production. However, it introduces several drawbacks. Firstly, the corrosive nature of high HF concentration can result in non-uniform morphology, including irregular thickness and surface roughness of the layers [Figure 3(b)], with oxidation of the metal 'Ti' to TiO_2 (2θ =25.4°) which can be evident from the XRD graph represented in Figure 3(a) [29].

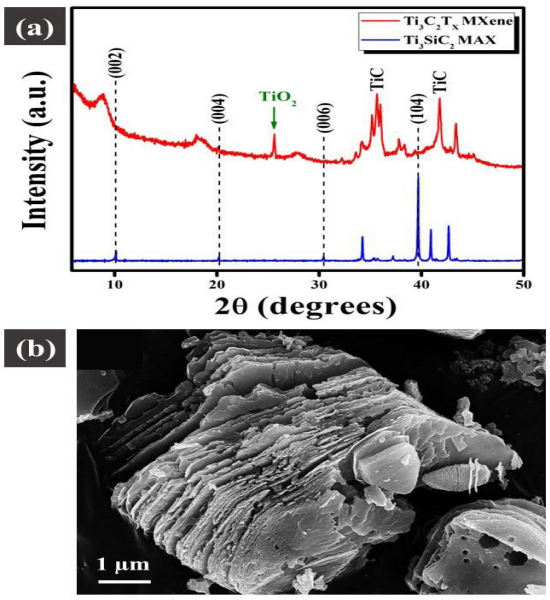

Figure 3. (a) X-ray diffraction pattern of Ti_3SiC_2 MAX phase (Blue) and its corresponding $Ti_3C_2T_x$ MXene (Red) showing formation of TiO_2 at 25.4°, (b) FESEM image of $Ti_3C_2T_x$ MXene showing surface roughness and broken layers.

This limits the MXene's applicability in certain downstream applications. Additionally, it increases the intrinsic defects such as single metal vacancies or vacancy clusters that reduces the quality of MXene layers.

Low etchant concentration

To avoid excessive etching and surface defects of the MXene layers, effect of low etchant (HF/H_2O_2) concentration on the synthesis of $Ti_3C_2T_x$ MXene from Ti_3SiC_2 MAX phase was studied. This condition resulted in slower etching rates, leading to prolonged synthesis time required to produce $Ti_3C_2T_x$ MXene. This sluggish etching process produced larger MXene flakes with a minimum concentration of defects and a larger oxygen to fluorine ratio [30]. However, this process hinders the complete removal of robust 'Si' layers from the Ti_3SiC_2 MAX phase, potentially resulting in incomplete transformation to $Ti_3C_2T_x$ MXene (Figure 4 a and b).

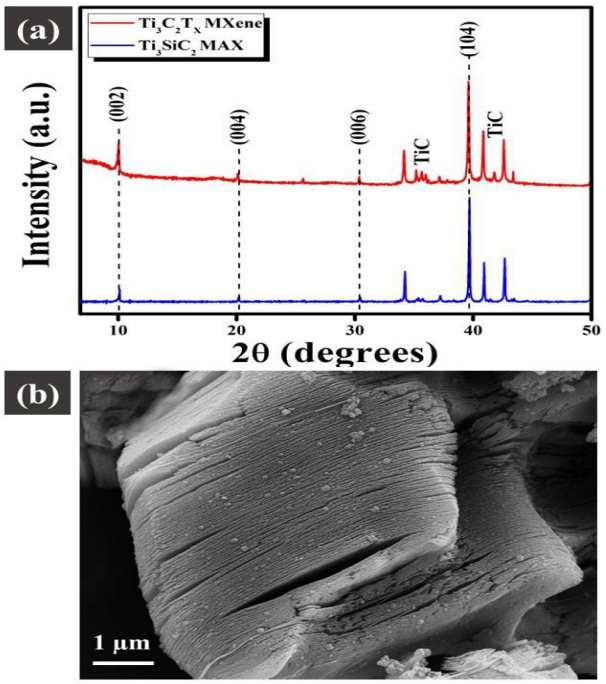

Figure 4. (a) X-ray diffraction pattern of Ti_3SiC_2 MAX phase (Blue) and its corresponding $Ti_3C_2T_x$ MXene (Red) showing no blue shift of (00l) peaks, (b) FESEM image of $Ti_3C_2T_x$ MXene showing compact MXene layers with few openings.

This can be evidenced from the XRD graph [Figure 4(a)] which shows no blue shift of the characteristic (00l) peaks of $Ti_3C_2T_x$ MXene. The FESEM micrograph represented in Figure 4(b) shows not well separated, compact layers of $Ti_3C_2T_x$ MXene which supports the XRD data. This impacts the material's properties such as electrical conductivity and mechanical strength. With subsequent optimization, high-quality $Ti_3C_2T_x$ MXene with high yield was achieved, which is described in section 2.2 of this article.

Characterization of Ti_3SiC_2 MAX phase and $Ti_3C_2T_x$ MXene

Powder X-ray diffraction (XRD) analysis

X-ray diffraction (XRD) analysis was employed to investigate the structural characteristics of the Ti_3SiC_2 MAX phase and its

https://doi.org/10.61577/jcti.2024.100008

corresponding $Ti_3C_2T_x$ MXene. Initially, the Ti_3SiC_2 MAX phase exhibited distinct peaks at 10.09°, 20.19°, 30.46°, 39.6° for the corresponding planes (002), (004), (006), and (104), respectively [25]. A small diffraction peak at ~36° confirms the formation of SiC as an impurity. However, there are no signs of TiC as an impurity which is evident from the graph. The disappearance of all diffraction peaks related to Ti_3SiC_2 MAX phase after acid etching was confirmed by the XRD pattern in Figure 5, indicating the formation of $Ti_3C_2T_x$ MXene. The shift of the characteristic (002) peak of $Ti_3C_2T_x$ MXene from 10.09° to 8.64° was observed, which confirmed the formation of the 2D layered structure, post-etching [26]. This transformation was further evidenced by changes in the interlayer spacing (from 8.74 Å to 10.08 Å), attributed to the introduction of surface terminations (-OH, -F, -O, etc.) during the etching process. This observation is consistent with previous literature reporting the blue shift of (00l) planes of $Ti_3C_2T_x$ MXene [31].

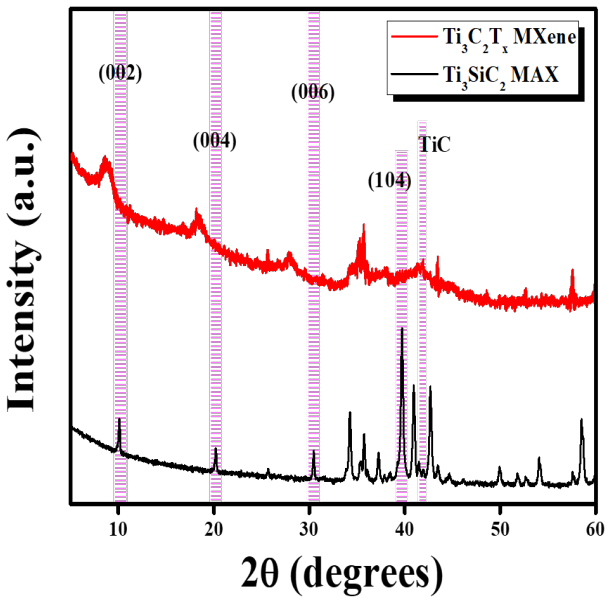

Figure 5. X-ray diffraction (XRD) spectra of Ti_3SiC_2 MAX phase (Black line) and it's corresponding $Ti_3C_2T_x$ MXene after etching (Red line).

Field-emission scanning electron microscopy (FESEM)

FESEM was used to examine the morphology of the Ti_3SiC_2 MAX phase and its derived $Ti_3C_2T_x$ MXene. As shown in Figure 6(a), the FESEM images of the Ti_3SiC_2 MAX phase reveal a closely packed laminated structure, typical of bulk-layered ternary carbides [32]. The presence of surface debris indicates impurities such as SiC with distinct morphologies. After acid etching, the Ti_3SiC_2 particles transformed into thin sheets with a well-defined accordion-like morphology, characteristic of multilayered $Ti_3C_2T_x$ MXene, as seen in Figure 6(b) [26,33]. This transformation indicates successful etching, where the Si layers are selectively removed, resulting in the exfoliation of the MAX phase into 2D MXene sheets. Elemental analysis (EDAX) (inset) of both samples confirms that the selective etching of the 'Si' layer from Ti_3SiC_2 MAX phase is achieved by the combined action of H_2O_2 and HF, leading to the development of surface terminations such as oxygen (-OH) and fluorine (-F), which make $Ti_3C_2T_x$ MXene nanosheets highly hydrophilic [34].

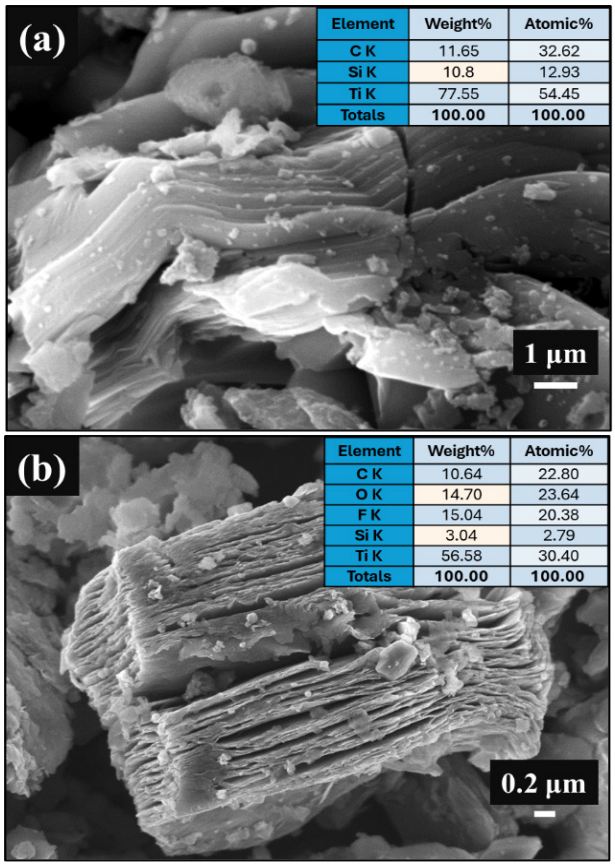

Figure 6. FESEM images of (a) Ti_3SiC_2 MAX phase showing typical compact layered structure, (b) well-defined accordion-like morphology of multi-layered $Ti_3C_2T_x$ MXene stack after etching in HF/H_2O_2. Inset showing EDAX of Ti_3SiC_2 MAX, $Ti_3C_2T_x$ MXene in figure (a) & (b), respectively.

Raman spectroscopy

This study utilizes Raman spectroscopy to assess the surface chemistry and quality of $Ti_3C_2T_x$ MXene nanosheets and to detect early signs of oxidation. The MXene Raman spectrum, shown in Figure 7, can be divided into several regions. The first is the resonant peak (125 cm^{-1}), observed with a 785 nm laser, which is coupled with the plasmonic peak. The next region is flake region from 150 cm^{-1} to 250 cm^{-1}. This area is characterized by the presence of A_{1g} (Ti,C,O) and E_g (Ti,C,O) vibrational modes which correspond to the in-plane and out-of-plane vibrational motions of the titanium atoms in the outer layer, as well as carbon and surface groups. A sharp resonant peak (Pink bands) at around 208 cm^{-1} corresponds to A_{1g} out-of-plane vibration of Ti, O, and C atoms in the flake region, while a similar peak at 725 cm^{-1} is due to the C-atoms in the carbon region. The region (Green band) from 230 to 470 cm^{-1} corresponds to in-plane (E_g) vibrations of surface groups attached to titanium atoms. This region is affected only by surface atoms, making it useful for studying the surface chemistry of MXenes and how it changes during chemical or electrochemical reactions. The region (Grey band) between 580 cm^{-1} and 730 cm^{-1} is primarily attributed to carbon vibrations (both E_g and A_{1g}) in the carbon region and is commonly used for fingerprinting surface groups in various in situ electrochemical studies [35].

https://doi.org/10.61577/jcti.2024.100008

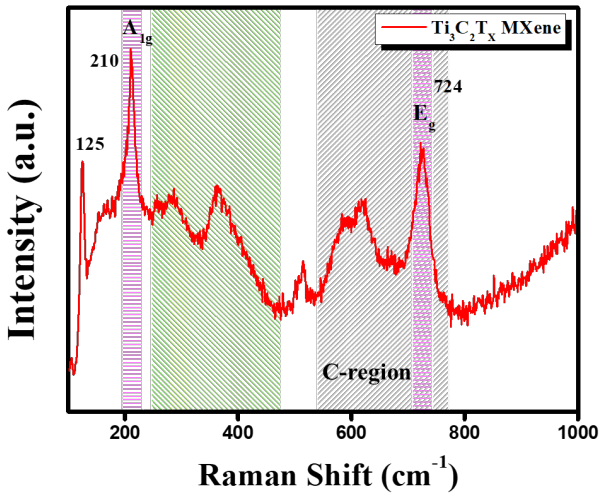

Figure 7. Raman spectrograph obtained from $Ti_3C_2T_x$ MXene powder and excited with 785 nm NIR laser. The spectrum shows out-of-plane vibration (pink bands) of Ti, C, O atoms in flake region and carbon region, E_g in-plane vibration (Green band) of surface groups, and carbon vibrations (both E_g and A_{1g}) in carbon region (Grey band).

Zeta potential of $Ti_3C_2T_x$ MXene

Figure 8 represents the zeta potential vs. pH graph of $Ti_3C_2T_x$ MXene nanosheets to determine the surface charge, which is an important factor for the success of the EPD process. Initially, the suspension's pH was slightly acidic (~6) due to negatively charged surface groups (-OH, -F, -O, etc.). The surface charge, measured with a zeta potential analyzer (Zetasizer Pro, Malvern Panalytical Ltd., UK) showed a negative potential of -35 mV at its natural pH, indicative of a stable colloidal dispersion. The pH was tuned by using 1M dilute sodium hydroxide (NaOH) and dilute nitric acid (HNO_3). Throughout the entire pH range, the zeta potential exhibited a decreasing trend with increasing pH, with minor fluctuations observed at pH 9, likely due to measurement error. At a pH of ~7.5, the $Ti_3C_2T_x$ MXene nanosheets exhibited maximum charge (-41 mV) with improved dispersibility which is suitable for carrying out the EPD process [36].

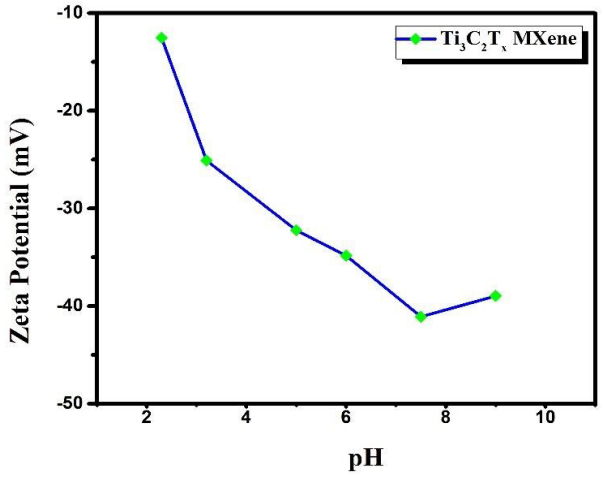

Figure 8. The plot represents the zeta potential of $Ti_3C_2T_x$ MXene at different pH.

Characterization of $Ti_3C_2T_x$ MXene coating on copper

Following the coating of $Ti_3C_2T_x$ MXene onto a copper substrate using EPD, as described in section 2.3, the material underwent detailed characterization and analysis to assess its morphological and electrochemical properties.

Field-emission scanning electron microscopy (FESEM)

Field-Emission Scanning Electron Microscopy (FESEM) was employed to analyze the morphological characteristics of $Ti_3C_2T_x$ MXene coatings deposited on copper substrates. Figure 9(a) depicts the micrograph of $Ti_3C_2T_x$ MXene on copper substrate, showing restacking of MXene layers during the drying or coating process. However, some needle-like structures were observed on the surface of $Ti_3C_2T_x$ MXene nanosheets. This could be primarily attributed to surface functionalization and hydrolysis, as well as chemical interactions of MXene functionalities with 1M dilute NaOH solution which was used during the EPD process. The addition of NaOH to the MXene suspension induces hydrolysis of surface functional groups, generating hydroxide ions (OH^-) that interact with the MXene surface, leading to significant ion adsorption. This interaction causes structural rearrangements and localized variations in surface energy, resulting in needle-like structures due to the crystallization or precipitation of reaction by-products, such as titanium hydroxide [$Ti(OH)_4$], which forms under alkaline conditions [37]. The elemental composition of the coating is elucidated through EDAX spectra (inset), which reveal the presence and relative abundance of constituent elements within the coating layer. Figure 9(b) illustrates the coated and uncoated areas of a single copper strip, highlighting the application of the protective coating. This visual evidence demonstrates the efficiency of the EPD process in uniformly depositing $Ti_3C_2T_x$ MXene onto the copper substrate. Additionally, the elemental mapping in Figure 9(c) reveals the spatial distribution of essential elements, including titanium (Ti), oxygen (O), and fluorine (F), across the coated surface.

Electrochemical analysis by Tafel polarization measurement

The electrochemical performance of $Ti_3C_2T_x$ MXene-coated copper (MXene/Cu) was evaluated using Tafel analysis to assess corrosion inhibition compared to bare copper. Before Tafel analysis, the samples were masked with epoxy, exposing a 1 cm^2 area, as illustrated in Figure 10(a). In a 3-electrode setup with Ag/AgCl as the reference and a Platinum wire as the counter electrode, the samples were treated as the working electrode, immersed in 3.5% NaCl at room temperature. Before running the Tafel analysis, open circuit potential (OCP) measurement was conducted which showed a positive shift from -0.211 V (bare Cu) to -0.019 V (MXene/Cu), indicating enhanced corrosion resistance [Figure 10(b)]. The Tafel polarization curves of the samples represented in Figure 10(c) revealed reduced I_{corr} values for MXene/Cu (0.27 μA/cm^2), compared to bare Cu (1533.20 μA/cm^2), with a calculated corrosion inhibition efficiency of 99.8%. This may be attributed to the formation of TiO_2 from low-valence 'Ti' states (Ti^{2+} and Ti^{3+}) in $Ti_3C_2T_x$ MXene, delaying metal oxidation [38]. OCP and Tafel values of both the samples are summarized in Table 2.

https://doi.org/10.61577/jcti.2024.100008

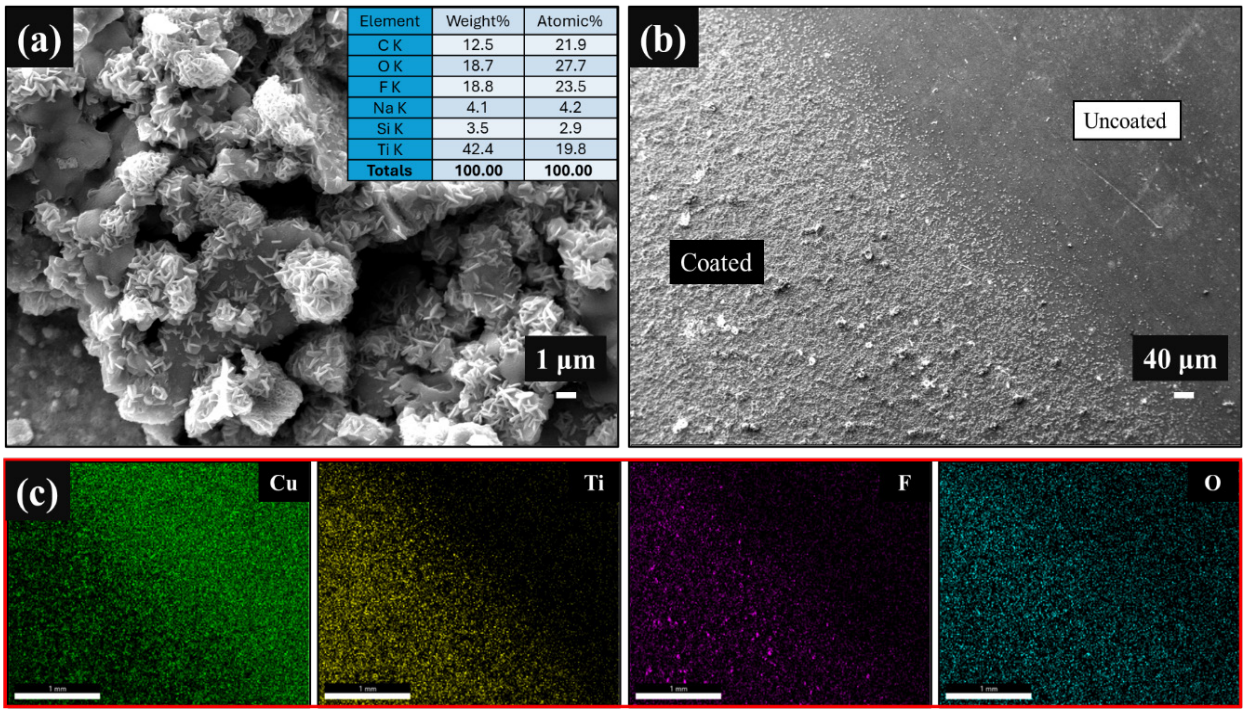

Figure 9. FESEM micrograph of (a) $Ti_3C_2T_x$ MXene coating on copper, showing restacked layers and needle-like structures due to interactions with dilute NaOH. Inset: EDAX spectra revealing the elemental composition of the coating, (b) Coated and uncoated regions of the copper strip, demonstrating the uniform deposition of $Ti_3C_2T_x$ MXene via the EPD process, (c) Elemental mapping of the coated copper surface, showing the distribution of Copper (Cu), Titanium (Ti), Oxygen (O), and Fluorine (F).

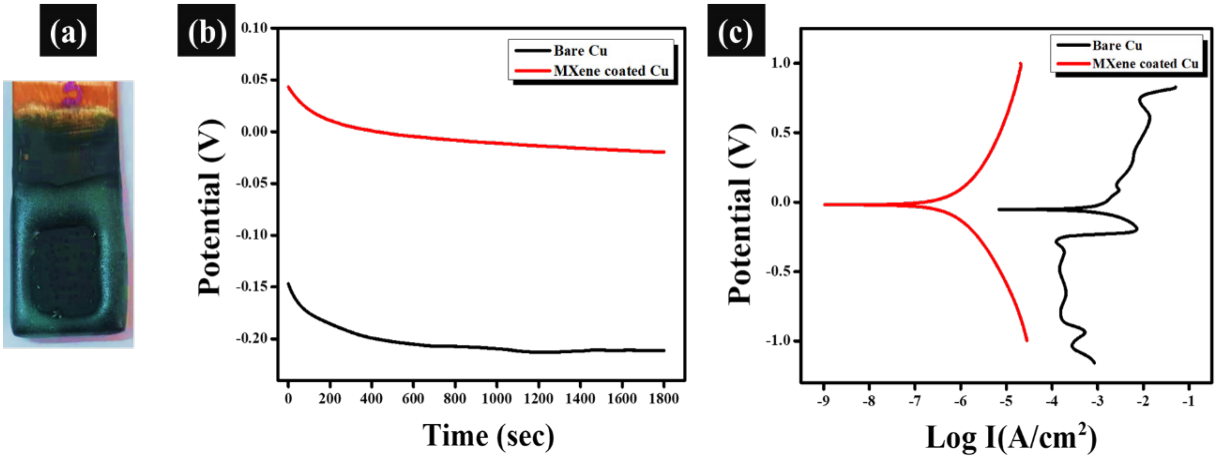

Figure 10. (a) $Ti_3C_2T_x$ MXene coated Cu substrate masked with epoxy, exposing 1 cm^2 area, (b) open circuit potential (OCP) measurements of bare Cu and MXene/Cu, (c) Tafel polarization curves of bare Cu and MXene/Cu carried-out in 3.5% NaCl at room temperature.

The corrosion inhibition efficiency () of the samples depicted in Table 2 were estimated by using the following equation 7.

$$\eta = \frac{I_{corr}(Bare\ Cu) - I_{corr}(Coated\ Cu)}{I_{corr}(Bare\ Cu)}\ x\ 100\% \quad [2]$$

Table 2. Electrochemical measurement values of bare Cu and MXene coated Cu.

Sample	OCP (V)	E_{corr} (V)	I_{corr} (µA/cm^2)	Corrosion Rate (mm/year)	η (%)
Bare Cu	-0.211	-0.054	1533.20	17.73	-
MXene/Cu	-0.019	-0.019	0.27	0.003	99.8%

https://doi.org/10.61577/jcti.2024.100008

The corrosion rate (CR) was determined using the following equation in accordance with the American Society for Testing and Materials (ASTM) standard G102 [39].

$$CR = K[I_{corr}/\sigma A] \; x \; EW \quad [3]$$

where, the corrosion rate constant (K)=3272 mm/year, the density (σ) of Cu=8.97 gm/cm3, the exposed surface area of the sample (A)=1 cm², and the equivalent weight (EW) of Cu=31.7 gm.

Conclusions

This study highlights the successful synthesis and application of high-quality $Ti_3C_2T_x$ MXene as a corrosion-resistant coating. Initially, the Ti_3SiC_2 MAX phase was synthesized with high purity through pressureless sintering by optimizing various parameters. $Ti_3C_2T_x$ MXene was then derived from MAX using a mixture of HF and H_2O_2 as etchants, with the concentration of the etchants playing a crucial role in producing high-quality MXene. Characterization techniques such as XRD and FESEM confirmed the formation of 2D layered $Ti_3C_2T_x$ MXene, with XRD showing a shift of the (002) peak from 10.09° to 8.64°, and FESEM revealing a well-separated, accordion-like structure. Raman spectroscopy provided insights into the surface chemistry and quality of the MXene nanosheets, identifying specific vibrational modes and early signs of oxidation. The zeta potential analysis indicated a maximum charge of -41 mV at pH ~7.5, confirming the effective surface functionalization. The synthesized MXene was coated onto copper substrates using electrophoretic deposition (EPD). FESEM and EDAX analyses demonstrated uniform coverage and significant surface functionalization of the MXene coatings. Electrochemical studies, including Tafel polarization and OCP measurements, revealed that the MXene-coated copper exhibited superior corrosion resistance, with a 99.8% corrosion inhibition efficiency. This enhanced performance is attributed to the formation of TiO_2 from low-valence Ti states (Ti^{2+} and Ti^{3+}) in the $Ti_3C_2T_x$ MXene, which delays metal oxidation.

These findings validate the potential of $Ti_3C_2T_x$ MXene as an effective corrosion-resistant coating, offering a promising approach for enhancing the longevity and durability of metal substrates. This work will be an added benefit to the electronic industries to prevent electrochemical corrosion where electrical conductivity and electromagnetic interference (EMI) shielding is an important factor.

Acknowledgment

This work was supported with the funding from Council of Scientific and Industrial Research (CSIR), India through the project HCP-0030. The authors thank the Central Characterization Department (CCD) of CSIR-Institute of Minerals and Materials Technology, Bhubaneswar for assistance in characterization techniques. The authors thank the Director, Institute of Minerals and Materials Technology, Bhubaneswar for permission to publish this paper.

Disclosure statement

No potential conflict of interest was reported by the authors.

References

1. Harsimran S, Santosh K, Rakesh K. Overview of corrosion and its control: A critical review. Proc Eng Sci. 2021;3(1):13-24. https://doi.org/10.24874/pes03.01.002
2. Bhaskaran R, Bhalla L, Rahman A, Juneja S, Sonik U, Kaur S, et al. An analysis of the updated cost of corrosion in India. Mater Perform. 2014;53(8):56-65. https://doi.org/10.1504/ijsom.2016.078891
3. Cui G, Bi Z, Wang S, Liu J, Xing X, Li Z, et al. A comprehensive review on smart anti-corrosive coatings. Prog Org Coat. 2020;148: 105821. https://doi.org/10.1016/j.porgcoat.2020.105821
4. He Y, Chen C, Xiao G, Zhong F, Wu Y, He Z. Improved corrosion protection of waterborne epoxy/graphene coating by combining non-covalent and covalent bonds. React Funct Polym. 2019;137: 104-115. https://doi.org/10.1016/j.reactfunctpolym.2019.02.001
5. Geim AK, Novoselov KS. The rise of graphene. Nat Mat. 2007;6(3):183-191. https://doi.org/10.1038/nmat1849
6. Ramezanzadeh B, Ghasemi E, Mahdavian M, Changizi E, Moghadam MM. Covalently-grafted graphene oxide nanosheets to improve barrier and corrosion protection properties of polyurethane coatings. Carbon. 2015;93;555–573. https://doi.org/10.1016/j.carbon.2015.05.094
7. Usha Kiran N, Dey S, Singh BP, Besra L. Graphene coating on copper by electrophoretic deposition for corrosion prevention. Coatings. 2017;7(12):214. https://doi.org/10.3390/coatings7120214
8. Spyrou K, Rudolf P. An Introduction to graphene. Functionalization of graphene. 2014:1-20 https://doi.org/10.1002/9783527672790.ch1
9. Boretti A, Al-Zubaidy S, Vaclavikova M, Al-Abri M, Castelletto S, Mikhalovsky S. Outlook for graphene-based desalination membranes. npj Clean Water. 2018;1(1):5. https://doi.org/10.1038/s41545-018-0004-z
10. Anasori B, Lukatskaya MR, Gogotsi Y. 2D metal carbides and nitrides (mxenes) for energy storage. Nat Rev Mater. 2017;2(2):1-7. https://doi.org/10.1038/natrevmats.2016.98
11. Dadashi Firouzjaei M, Nemani SK, Sadrzadeh M, Wujcik EK, Elliott M, Anasori B. Life-cycle assessment of ti3c2tx mxene synthesis. Adv Mater. 2023;35(31):2300422. https://doi.org/10.1002/adma.202300422
12. Anasori B, Gogotsi ÜG. 2D metal carbides and nitrides (MXenes). Springer. 2019;416. https://doi.org/10.1007/978-3-030-19026-2_1
13. Huang H, Sheng X, Tian Y, Zhang L, Chen Y, Zhang X. Two-dimensional nanomaterials for anticorrosive polymeric coatings: A review. Ind Eng Chem Res. 2020;59(35):15424-15446. https://doi.org/10.1021/acs.iecr.0c02876
14. Butt MA. Thin-film coating methods: A successful marriage of high-quality and cost-effectiveness—a brief exploration. Coatings. 2022;12(8):1115. https://doi.org/10.3390/coatings12081115
15. Yan H, Li W, Li H, Fan X, Zhu M. Ti3C2 MXene nanosheets toward high-performance corrosion inhibitor for epoxy coating. Prog Org Coat. 2019;135:156-167. https://doi.org/10.1016/j.porgcoat.2019.06.013
16. Zhao H, Ding J, Zhou M, Yu H. Air-stable titanium carbide mxene nanosheets for corrosion protection. ACS Appl Nano Mater. 2021;4(3):3075-3086. https://doi.org/10.1021/acsanm.1c00219
17. Li S, Huang H, Chen F, He X, Ma Y, Zhang L, Sheng X, Chen Y, Shchukina E, Shchukin D. Reinforced anticorrosion performance of waterborne epoxy coating with eco-friendly l-cysteine modified ti3c2tx mxene nanosheets. Prog Org Coat. 2021;161:106478.
18. Shi K, Meng X, Xiao S, Chen G, Wu H, Zhou C, Jiang S, Chu PK. MXene coatings: Novel hydrogen permeation barriers for pipe steels. Nanomaterials. 2021;11(10):2737. https://doi.org/10.3390/nano11102737
19. Xu S, Wei G, Li J, Ji Y, Klyui N, Izotov V, Han W. Binder-free $Ti_3C_2T_x$ MXene electrode film for supercapacitor produced by electrophoretic deposition method. Chem Eng J. 2017;317: 1026-1036. https://doi.org/10.3390/nano11102737
20. Wang K, Zheng B, Mackinder M, Baule N, Garratt E, Jin H, Schuelke T, Fan QH. Efficient electrophoretic deposition of mxene/reduced graphene oxide flexible electrodes for all-solid-state supercapacitors. J Energy Storage. 2021;33:102070. https://doi.org/10.1016/j.est.2020.102070
21. Deng J, Lu Z, Ding L, Li ZK, Wei Y, Caro J, Wang H. Fast electrophoretic preparation of large-area two-dimensional titanium carbide membranes for ion sieving. Chem Eng J. 2021;408:127806.

https://doi.org/10.61577/jcti.2024.100008

https://doi.org/10.1016/j.cej.2020.127806
22. Jang JH, Oh JS, Lee EJ, Han CM. Electophoretically deposition of ti3c2 on titanium surface for hard tissue implant applications. Coatings. 2021;11(7):761. https://doi.org/10.3390/coatings11070761
23. Namvari M, Chakrabarti BK. Electrophoretic deposition of mxenes and their composites: Toward a scalable approach. Advances in Colloid and Interface Science. 2024;103208. https://doi.org/10.1016/j.cis.2024.103208
24. Han M, Yin X, Wu H, Hou Z, Song C, Li X, Zhang L, Cheng L. Ti3C2 MXenes with Modified Surface for High-Performance Electromagnetic Absorption and Shielding in the X-Band. ACS applied materials & interfaces. 2016;8(32):21011-21019. https://doi.org/10.1021/acsami.6b06455
25. Kiran NU, Das P, Chatterjee S, Besra L. Effect of 'Ti' particle size in the synthesis of highly pure Ti_3SiC_2 MAX phase. Nano-Struct Nano-Objects. 2022;30:100849. https://doi.org/10.1016/j.nanoso.2022.100849
26. Kiran NU, Deore AB, More MA, Late DJ, Rout CS, Mane P, et al. Comparative study of cold electron emission from 2D $Ti_3C_2T_x$ MXene nanosheets with respect to its precursor Ti_3SiC_2 MAX phase. ACS Appl Electron Mater. 2022;4(6):2656-2666. https://doi.org/10.1021/acsaelm.2c00128
27. Zhang CJ, Pinilla S, McEvoy N, Cullen CP, Anasori B, Long E, et al. Oxidation stability of colloidal two-dimensional titanium carbides (MXenes). Chemistry of Materials. 2017;29(11):4848-4856. https://doi.org/10.1021/acs.chemmater.7b00745
28. Ho-Duc LH. Synthesis and characterization of the properties of Ti_3SiC_2/SiC and Ti_3SiC_2/TiC Composites. 2002. https://doi.org/10.17918/etd-54
29. Wang S, Liu Y, Liu Y, Hu W. Effect of HF etching on titanium carbide ($Ti_3C_2T_x$) microstructure and its capacitive properties. Chem Eng J. 2023;452:139512. https://doi.org/10.1016/j.cej.2022.139512
30. Munir S, Rasheed A, Rasheed T, Ayman I, Ajmal S, Rehman A, et al. Exploring the influence of critical parameters for the effective synthesis of high-quality 2D MXene. ACS Omega. 2020;5(41): 26845-26854. https://doi.org/10.1021/acsomega.0c03970
31. Alhabeb M, Maleski K, Anasori B, Lelyukh P, Clark L, Sin S, Gogotsi Y. Guidelines for synthesis and processing of two-dimensional titanium carbide (Ti_3C_2T x MXene). Chem Mater. 2017;29(18): 7633-7644. https://doi.org/10.1021/acs.chemmater.7b02847
32. Barsoum MW, El-Raghy T. Synthesis and characterization of a remarkable ceramic: Ti_3SiC_2. J Am Ceram Soc. 1996;79(7): 1953-1956. https://doi.org/10.1111/j.1151-2916.1996.tb08018.x
33. Naguib M, Kurtoglu M, Presser V, Lu J, Niu J, Heon M, Hultman L, Gogotsi Y, Barsoum MW. Two-dimensional Nanocrystals Produced by Exfoliation of Ti3AlC2. Adv Mater. 2011;23(37):4248-4253. https://doi.org/10.1002/adma.201190147
34. Alhabeb M, Maleski K, Mathis TS, Sarycheva A, Hatter CB, Uzun S, et al. Selective etching of silicon from Ti_3SiC_2 (MAX) to obtain 2D titanium carbide (MXene). Angewandte Chemie. 2018;130(19): 5542-5546. https://doi.org/10.1002/ange.201802232
35. Sarycheva A, Gogotsi Y. Raman spectroscopy analysis of the structure and surface chemistry of $Ti_3C_2T_x$ MXene. Chem Mater. 2020;32(8):3480-3488. https://doi.org/10.1021/acs.chemmater.0c00359
36. Li Y, Zhou X, Wang J, Deng Q, Li M, Du S, et al. Facile preparation of in situ coated $Ti_3C_2T_x$/Ni 0.5 Zn 0.5 Fe2O4 composites and their electromagnetic performance. Rsc Adv. 2017;7(40):24698-24708. https://doi.org/10.1039/c7ra03402d
37. Alkanad K, Hezam A, Al-Zaqri N, Bajiri MA, Alnaggar G, Drmosh QA, et al. One-step hydrothermal synthesis of anatase TiO2 nanotubes for efficient photocatalytic CO2 Reduction. ACS Omega. 2022;7(43):38686-38699. https://doi.org/10.1021/acsomega.2c04211
38. Zhang F, Liu W, Wang S, Shi H, Liu C, Liang L, et al. Engineering MXenes ($Ti_3C_2T_x$) surface with TiO2 for enhancing anti-corrosion performance of coatings. Polymer. 2021;230:124086. https://doi.org/10.1016/j.polymer.2021.124086
39. Astm G. Standard practice for calculation of corrosion rates and related information from electrochemical measurements. G102-89. 2004. https://doi.org/10.1520/g0102-89r04e01

https://doi.org/10.61577/jcti.2024.100008